The Future Intensification of the North Atlantic Winter Storm Track: The Key Role of Dynamic Ocean Coupling

REI CHEMKE,[a] LAURE ZANNA,[b] CLARA ORBE,[c] LORI T. SENTMAN,[d] AND LORENZO M. POLVANI[e,f,g]

[a] *Department of Earth and Planetary Sciences, Weizmann Institute of Science, Rehovot, Israel*
[b] *Courant Institute of Mathematical Sciences, New York University, New York, New York*
[c] *NASA Goddard Institute for Space Studies, New York, New York*
[d] *NOAA/Geophysical Fluid Dynamics Laboratory, Princeton, New Jersey*
[e] *Department of Applied Physics and Applied Mathematics, Columbia University, New York, New York*
[f] *Department of Earth and Environmental Sciences, Columbia University, New York, New York*
[g] *Lamont-Doherty Earth Observatory, Columbia University, New York, New York*

ABSTRACT: Climate models project an intensification of the wintertime North Atlantic Ocean storm track, over its downstream region, by the end of this century. Previous studies have suggested that ocean–atmosphere coupling plays a key role in this intensification, but the precise role of the different components of the coupling has not been explored and quantified. In this paper, using a hierarchy of ocean coupling experiments, we isolate and quantify the respective roles of thermodynamic (changes in surface heat fluxes) and dynamic (changes in ocean heat flux convergence) ocean coupling in the projected intensification of North Atlantic transient eddy kinetic energy (TEKE). We show that dynamic coupling accounts for nearly all of the future TEKE strengthening as it overcomes the much smaller effect of surface heat flux changes to weaken the TEKE. We further show that by reducing the Arctic amplification in the North Atlantic, ocean heat flux convergence increases the meridional temperature gradient aloft, causing a larger eddy growth rate and resulting in the strengthening of North Atlantic TEKE. Our results stress the importance of better monitoring and investigating the changes in ocean heat transport, for improving climate change adaptation strategies.

SIGNIFICANCE STATEMENT: By the end of this century, the North Atlantic Ocean storm track is projected to intensify on its eastward flank. Such intensification will have large societal impacts, mostly over western Europe. Thus, it is critical to better understand the mechanism underlying the intensification of the storm track. Here we investigate the role of ocean coupling in the future intensification of the North Atlantic storm track and find that ocean heat transport processes are responsible for the strengthening of the storm track. Our results suggest that better monitoring the changes in ocean heat transport will hopefully improve climate change adaption strategies.

KEYWORDS: Atmosphere–ocean interaction; Dynamics; Eddies; Large-scale motions; General circulation models

---

1. Introduction

Midlatitude storms play a central role in the weather and climate of the extratropics. These storms not only modulate the temperature, precipitation, and winds over synoptic time scales, they also account for most of the energy (i.e., heat, moisture, and momentum) transport from low to high latitudes, and across longitudes, over multidecadal time scales. It is thus important to investigate the mechanisms associated with the midlatitude storms' response to anthropogenic emissions.

In the Southern Hemisphere, climate models project a poleward shift of midlatitude summer storm tracks, and an intensification of winter storm tracks. In the Northern Hemisphere, summer storm tracks are projected to weaken by the end of this century, while winter storm tracks to strengthen, mostly over the downstream region of the North Atlantic storm track (Chang et al. 2012; Zappa et al. 2013; Harvey et al. 2014; Lehmann et al. 2014; Harvey et al. 2020). This eastward extension of the North Atlantic storm track has great societal impacts, especially over western Europe (Zappa et al. 2013). It should be noted that previous studies have found different magnitudes of the future North Atlantic storm-track intensification, in part due to the different metrics used to define the storm track. For example, while a robust strengthening of the storm track was found using Eulerian metrics such as eddy variances (mostly at upper levels; Chang et al. 2012; Coumou et al. 2015) and sea level pressure (Harvey et al. 2014, 2020), a weaker strengthening of North Atlantic storm track was found using cyclone tracking algorithms (Zappa et al. 2013).

Previous studies argued for the importance of ocean–atmosphere coupling in modulating the North Atlantic Ocean winter storm track (Magnusdottir et al. 2004; Brayshaw et al. 2011). For example, variations in the Atlantic meridional overturning circulation (AMOC) and North Atlantic gyres were argued to modify the seasonal to decadal variability of the North Atlantic storm track, via changes in sea surface temperature (SST) (Frankignoul et al. 2013; Gastineau et al. 2013). Over longer time

scales, the future changes, by the end of the twenty-first century, in winter SST were argued to account for most of the intensification of the North Atlantic storm track (Ciasto et al. 2016) (whether this is a remote or local effect of the SST is still under debate; Ciasto et al. 2016; Gervais et al. 2019). In particular, ocean dynamical changes (i.e., changes in ocean heat transport/uptake) were suggested to affect the intensification of the North Atlantic storm track. In response to anthropogenic emissions, the AMOC was argued, based on a regression analysis, to modulate the intensification of the North Atlantic winter storm track across phase 3 of the Coupled Model Intercomparison Project (CMIP3) (Woollings et al. 2012), and similarly, to modulate the jet's position across CMIP5 and CMIP6 models (Bellomo et al. 2021).

To further investigate the role of ocean heat transport changes in the North Atlantic storm track's response to anthropogenic emission, Woollings et al. (2012) used fixed ocean-heat-transport experiments: the projected storm track's response by 2100 under the 20C3M and SRESA1B forcing scenarios, using fully coupled models with active ocean heat transport, was compared with the storm track's response to doubling of CO_2 concentrations, using slab ocean models with fixed ocean heat transport. Changes in ocean heat transport were mostly argued to contribute to the southward shift of the downstream region of the North Atlantic storm track, but not to the intensification of the storm track. Woollings et al. (2012), therefore, suggested that the role of the AMOC in the storm track's response is overcome by other ocean heat transport processes.

The use of different forcings (future transient scenarios vs equilibrated $2 \times CO_2$ concentrations) in the above experiments might have prevented Woollings et al. (2012) from fully quantifying the role of ocean heat transport changes in the storm track's response to anthropogenic emissions; the different storm-track responses in the fully coupled and fixed ocean-heat-transport experiments might not only stem from the presence/absence of ocean heat transport changes but from the use of different forcings as well (Fig. S1 in the online supplemental material). Thus, the aim of this study is to quantify the role of ocean coupling, and in particular of ocean heat transport/uptake, in the intensification of the North Atlantic winter storm track by the end of this century (note that here we focus on the large-scale atmospheric response, and not on the interaction of individual storms with the ocean; Czaja et al. 2019). Not only do we quantify the role of ocean coupling in the storm track's intensification, but we also elucidate the mechanism underlying the effect of ocean coupling on the North Atlantic storm track. To accomplish this, we build on previous fixed-ocean-coupling studies (Deser et al. 2016; Chemke and Polvani 2018; Chemke et al. 2019; Chemke 2021; Chemke et al. 2021) and construct a hierarchy of ocean coupling experiments in large ensembles of model simulations forced by twentieth and twenty-first-century forcings.

2. Methods

a. North Atlantic transient eddy kinetic energy

Following previous studies (O'Gorman and Schneider 2008; Chang et al. 2012; Coumou et al. 2015; Chemke and Ming 2020) we estimate the intensity of the North Atlantic winter storm track through use of the December–February (DJF) vertically integrated transient eddy kinetic energy (TEKE),

$$\text{TEKE} = \frac{1}{g} \int_0^{p_s} \left(\overline{u'^2} + \overline{v'^2} \right) dp,$$

where g is gravity, p_s is surface pressure; p is pressure; u and v are the zonal and meridional winds, respectively; and prime denotes deviation from monthly mean (denoted by overbar). We here define the eddies as deviations from monthly mean since only monthly data of kinetic energy is available from the hierarchy of ocean coupling experiments used in this study. Nevertheless, the intensification of the North Atlantic winter storm track, found using a high bandpass filter (e.g., 2–6 days) in previous studies (see also Fig. S2 in the online supplemental material), is also clearly evident using deviations from monthly mean, as shown below. In addition, we define the downstream region of the storm track over the region, 60°W–30°E and 40°–60°N, where most of the strengthening of the storm track occurs by the end of the twenty-first century (green boxes in Figs. 3a and 4a).

b. CMIP5 models

We analyze daily output of zonal and meridional winds from 14 CMIP5 models (Taylor et al. 2012) (BCC_CSM.1, BNU-ESM, CanESM2, CMCC-CMS, FGOALS-g2, FGOALS-s2, GFDL CM3, GFDL-ESM2G, GFDL-ESM2M, IPSL-CM5A-LR, IPSL-CM5B-LR, MIROC-ESM, MIROC-ESM-CHEM, and MPI-ESM-MR), which were integrated between 1850 and 2100 under the historical and representative concentration pathway 8.5 (RCP8.5) forcings (Riahi et al. 2011). For simplicity, we here use only the r1i1p1 realization in each model.

c. Hierarchy of ocean coupling experiments

To quantify and elucidate the role of ocean coupling in the future North Atlantic TEKE changes (by the end of this century), we use the Community Earth System Model (CESM1) (Hurrell et al. 2013) and analyze a hierarchy of ocean coupling experiments in three large ensembles of model integrations. The CESM1 comprises the Community Atmosphere Model, version 5.3 (CAM V5.3); version 4 of the Los Alamos Sea Ice Model (CICE4); Los Alamos Parallel Ocean Program, version 2 (POP2); and Community Land Model, version 4. Each ensemble includes a different ocean model component (full-physics or slab-ocean), and their combination elucidates the roles of different oceanic coupling processes in the North Atlantic TEKE response to anthropogenic emissions. Ocean coupling processes can be investigated via the mixed layer temperature equation, which takes the simple form

$$\rho c_p h \frac{\partial T}{\partial t} = \text{SHF} + \text{OHFC},$$

where ρ is seawater density, c_p is the ocean specific heat capacity, h is the mixed layer depth, T is the mixed layer temperature, SHF represents the net heat flux into the ocean from both atmosphere and sea ice (surface heat fluxes), and
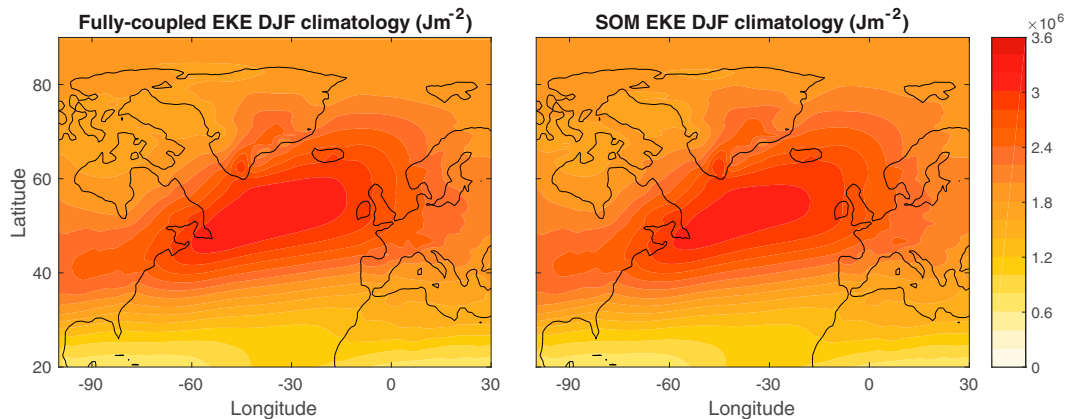
FIG. 1. Preindustrial climatology of DJF TEKE in the (left) fully coupled and (right) slab ocean models of the CESM1.

OHFC is the ocean heat flux convergence in the mixed layer $[-\nabla \cdot (vT)$, including both horizontal and vertical heat fluxes].

The first large ensemble (LE) is fully coupled and described in Kay et al. (2015) and consists of 40 members running from 1920 to 2100 under the same historical and RCP8.5 forcings as in CMIP5. The first member of the ensemble is initialized from a long preindustrial control run and at 1920, all other members branch off the first member using a minor change in air temperature $[O(10^{-14} \text{ K})]$. Thus, the LE allows investigating the transient forced response of the system to external forcings, as the ensemble mean averages out the internal variability. Since the full-physics ocean model is used in LE, ocean coupling (i.e., ocean–atmosphere and ocean–sea ice processes are active) can affect the TEKE response to external forcings over the twentieth and twenty-first centuries.

The second ensemble consists of 20 members and has the same atmosphere, land and sea ice model components as the LE but a different ocean component: the full-physics ocean model is replaced with a slab ocean model. In the slab ocean model ensemble (SOM LE) the OHFC and mixed layer depth vary spatially, but are fixed to monthly and annual values, respectively (i.e., fixed dynamic coupling), calculated from the climatology of a long preindustrial control run using the fully coupled model (as described in Bitz et al. (2012), the OHFC is calculated monthly from the mixed layer temperature equation, and averaged over 1100 years). Thus, in SOM LE, changes in ocean horizontal heat transport and vertical heat uptake by the deep ocean (note that the mixed layer depth is also fixed as it accounts for part of the vertical heat mixing) cannot affect the TEKE response to anthropogenic emissions. Comparing the response in LE and SOM LE isolates, and thus enables quantifying, the role of OHFC changes, including both horizontal heat transport and vertical heat uptake by the deep ocean (vertical heat transfer via diffusion/convection/advection) in the TEKE response. Note that the dynamic coupling component accounts for the impacts of OHFC and not only the impacts of the oceanic circulation.

A few clarifications on the SOM LE. First, the sea ice component, that is, the dynamic–thermodynamic sea ice model, CICE4, may affect the mixed layer temperature via latent and sensible heat fluxes associated with open-ocean snowfall and sea ice growth, surface lateral and basal fluxes and ice runoff (Bitz et al. 2012). Second, since the OHFC and mixed layer depth in SOM LE are calculated from the preindustrial run of the fully coupled model, the two ensembles are initialized from a very similar background state (Fig. 1); the differences between the background states of the TEKE in the two simulations are statistically insignificant and of almost two orders of magnitude smaller than the TEKE climatology (Fig. S3 in the online supplemental material). Last, the SOM LE is constructed in the same way as LE: the first member is initialized from a long preindustrial control run of 900 yr, and all other members branch off the first member at 1920, and run from 1920 to 2100 (under the same forcings as in LE).

For consistency with the large body of work done on the role of SST in the climate's response to increased greenhouse gases using atmosphere-only runs (e.g., Ciasto et al. 2016), the third ensemble is similar to SOM LE (consists of 20 members using the slab ocean model of CESM1 forced under the historical and RCP8.5 forcings) except for the mixed layer temperature, which varies spatially, but is fixed to its monthly preindustrial values (including below the sea ice). Thus, in this ensemble there is no active ocean model (NOM LE), as both OHFC and SHF cannot affect the TEKE response. Comparing the TEKE response in LE and NOM LE isolates the role of net ocean coupling over the twentieth and twenty-first centuries (ocean–atmosphere and ocean–sea ice coupling). Note that the NOM LE runs are slightly different than atmosphere-only runs, where both SST and sea ice are fixed, since in NOM LE only the SST is prescribed (here to preindustrial values). This allows isolating only the net role of ocean coupling, without the effect of sea ice–atmosphere interactions, although this effect is likely minor (note that the sea ice in NOM LE is treated as in SOM LE).

Furthermore, comparing the TEKE response in SOM LE and NOM LE isolates the effect of SHF, because this process is active in SOM LE but not in NOM LE. Following previous studies (e.g., Deser et al. 2016), we refer to the SHF (i.e., the impact of ocean–atmosphere and ocean–sea ice heat fluxes on the mixed layer temperature) as thermodynamic ocean
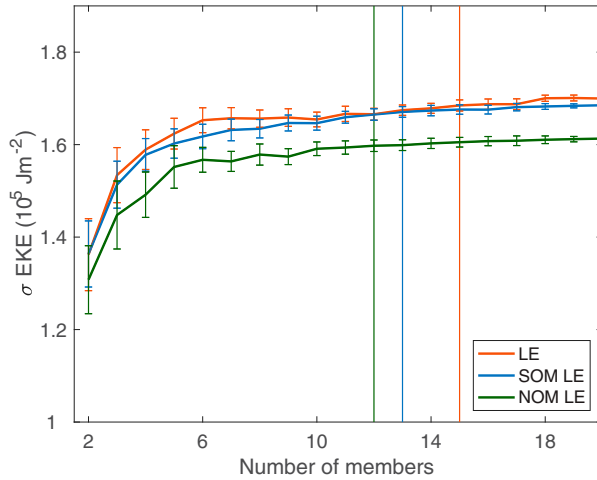
FIG. 2. One standard deviation of DJF North Atlantic TEKE, over the downstream region of the storm track, across different numbers of ensemble members. The standard deviation is calculated each year, and averaged over the 1920–2100 period, and over all combinations of number of ensemble members (or up to 1000 random combinations) in LE (red), SOM LE (blue), and NOM LE (green). Error bars show the standard deviation across the different combinations of number of ensemble members. Vertical lines show the number of members that capture 99% of the TEKE variability across all members.

coupling. Thus, by construction, the sum of the difference between LE and SOM LE and the difference between SOM LE and NOM LE yields the net effect of ocean coupling (i.e., the difference between LE and NOM LE); such decomposition allows one to investigate the different processes that modulate the SST response (i.e., the SHF and OHFC in the mixed layer equation), as inferred from the fixed SST runs.

Last, we verify that each ensemble is sufficiently large to capture the variability of North Atlantic TEKE over the downstream region of the storm track by calculating the TEKE variability (defined as one standard deviation of inter-member spread) across different number of ensemble members n. In particular, we calculate the standard deviation in each combination of ensemble members (or up to 1000 random combinations) of size n and average over all combinations. This is done for each year over the 1920–2100 period, and the mean over all years is shown in Fig. 2. Figure 2 shows that 12, 13, and 15 members in NOM LE, SOM LE, and LE, respectively, already capture 99% (marked by the vertical lines) of the TEKE variability in the ensembles (the 0.99 ratio between standard deviations across n members and across all members). Thus, the size of each ensemble is sufficiently large to capture the variability and forced response of North Atlantic TEKE.

d. Ocean heat flux convergence experiments under idealized forcing

To ensure that the role of OHFC in the TEKE response to anthropogenic emissions in CESM1 is robust and evident in other models, we also analyze fixed-OHFC experiments in

two other models: the NASA Goddard Institute for Space Studies Model E2.1 (GISS Model E2.1) (Kelley et al. 2020), and the Geophysical Fluid Dynamics Laboratory's CM4.0 (GFDL CM4) (Held et al. 2019). Similar to the ocean experiments in CESM1, we make use of the fully coupled and slab ocean versions of the GISS Model E2.1 and GFDL CM4, only here forced by an abrupt quadrupling of CO_2 concentrations, relative to preindustrial values; the slab ocean models have fixed OHFC and mixed layer depth, and the same dynamic–thermodynamic sea ice model as in the fully coupled models. This allows us to qualitatively verify the results from CESM1, as CO_2 concentrations, in the RCP8.5 scenario, are expected to approximately quadruple by the end of this century. For the fully coupled and slab ocean models in GISS Model E2.1 we use the last 40 years of 150- and 60-yr runs, respectively. In GFDL CM4, we use the last 40 years of a 150-yr run in both the slab ocean and fully coupled models. We also examine the TEKE response to abrupt doubling and quadrupling of CO_2 concentrations using the last 40 years of a 150-yr run of the fully coupled and slab ocean versions of CESM1. This allows us to examine the effect of different forcings on the role of OHFC in the TEKE response. Note that corresponding NOM simulations are not available from these models.

e. Linear normal mode instability analysis

To investigate the mechanism underlying the role of ocean coupling in the projected changes of North Atlantic TEKE, we follow previous studies (e.g., Smith 2007; Chemke and Polvani 2019; Chemke and Ming 2020) and apply a linear normal-mode instability analysis to the quasigeostrophic equations over the North Atlantic region in the hierarchy of ocean coupling experiments. This analysis allows us to examine the growth rate of the North Atlantic storm track, which is a widely used metric for the baroclinicity of the flow, that is, the extraction of energy, by the eddies, from the mean flow. The quasigeostrophic equations, linearized about a mean state, can be written as follows:

$$\frac{\partial q'}{\partial t} + \overline{\mathbf{u}} \cdot \nabla q' + \mathbf{u}' \cdot \nabla \overline{q} = 0, \quad p_{\text{trop}} < p < p_s, \text{and}$$

$$\frac{\partial}{\partial t}\frac{\partial \psi'}{\partial p} + \overline{\mathbf{u}} \cdot \nabla \frac{\partial \psi'}{\partial p} + \mathbf{u}' \cdot \nabla \frac{\partial \overline{\psi}}{\partial p} = 0, \quad p = p_{\text{trop}}, p_s, \quad (1)$$

where the first equation is derived from the conservation of quasigeostrophic potential vorticity q at the interior and the second is derived from conservation of potential temperature θ at the surface and tropopause height p_{trop}. The quasigeostrophic eddy potential vorticity can be written as $q' = \nabla^2 \psi' + \Gamma \psi'$, where $\psi = \phi/f$ is the streamfunction, ϕ is the geopotential, f is the Coriolis parameter,

$$\Gamma = \frac{\partial}{\partial p}\frac{f^2}{S^2}\frac{\partial}{\partial p}$$

is a second-order differential operator,

$$S^2 = -\frac{1}{\overline{\rho}\,\overline{\theta}}\frac{\partial \overline{\theta}}{\partial p}$$
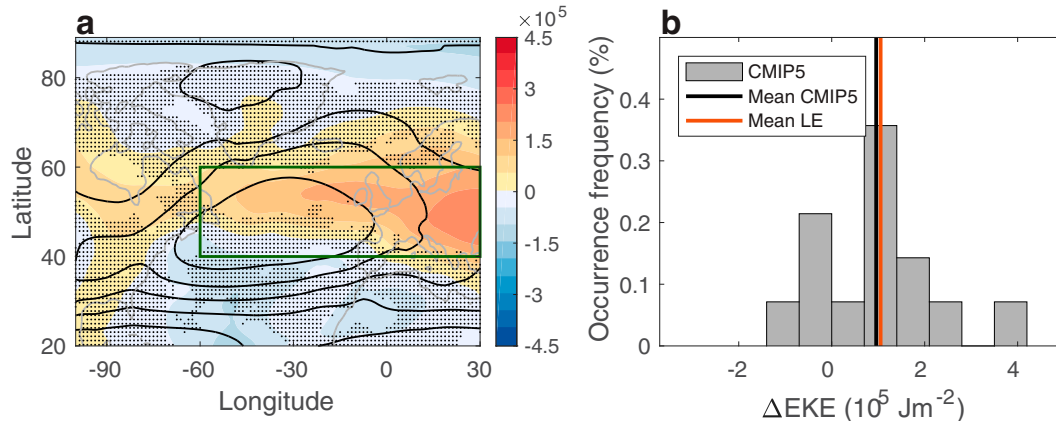
FIG. 3. (a) The response to anthropogenic emissions (difference between the last 20 years of the twenty-first and twentieth centuries) of DJF North Atlantic TEKE (J m^{-2}) in CMIP5 mean (shading). Black contours show the TEKE averaged over the last 20 years of the twentieth century in intervals of 3×10^5 J m^{-2}, with a maximum value of 2.2×10^6 J m^{-2}. Stippling shows where less than two-thirds of the models agree on the sign of change. The green-outlined box shows the downstream region of the storm track. (b) The occurrence frequency of the TEKE response (10^5 J m^{-2}) averaged over the downstream region of the storm track in CMIP5 models (gray bars). Vertical black and red lines show the CMIP5 mean and LE mean, respectively. One standard deviation across the LE members is 6.2×10^4 J m^{-2}.

is static stability, and ρ is density. The mean quasigeostrophic potential vorticity gradient is defined as

$$\nabla \overline{q} = \Gamma \overline{v} \hat{i} + (\beta - \Gamma \overline{u}) \hat{j},$$

where β is the meridional derivative of f and

$$\nabla \frac{\partial \overline{\psi}}{\partial p} = \frac{\partial \overline{v}}{\partial p} \hat{i} - \frac{\partial \overline{u}}{\partial p} \hat{j}.$$

Transforming Eq. (1) to an eigenvalue problem, using a plane-wave solution,

$$\psi' = \mathrm{Re}\left[\hat{\psi}'(p) e^{i(kx - \omega t)}\right],$$

allows one to explore the growth rate of the waves (using all model levels between p_s to p_{trop}), which is represented by the imaginary component of the frequency ω (the eigenvalue); we here analyze the fastest growth rate. The input for the eigenvalue problem is the mean North Atlantic wintertime fields (i.e., temperature, zonal wind, and tropopause height) from each ensemble, averaged over the downstream region of the storm track (calculating the growth rate over the upstream region of the storm track, does not allow the growth rate to capture the TEKE response over the downstream region).

The linear normal mode instability analysis allows one to account for the vertical variations in the zonal wind shear and static stability changes, which are usually overlooked when using a more simplified metric of the growth rate, such as the Eady growth rate. These variations play an important role in the effects of ocean coupling on the North Atlantic TEKE response (as shown below). Last, note that while the above analysis accounts for the effects of the mean flow on the eddies, it does not account for the effects of the eddies on the mean flow.

f. Student's t test

For estimating the significance of the response of different fields to anthropogenic emissions (i.e., the difference between the 2080–99 and 1980–99 periods), and the difference between the different ensembles, we here use an independent two-sample t test (Deser et al. 2012).

3. Results

a. Quantifying the role of ocean coupling in the projected response of North Atlantic TEKE to anthropogenic emissions

We start by considering the response to anthropogenic emissions (difference between the last 20 years of the twenty-first and twentieth centuries) of DJF North Atlantic TEKE in CMIP5 models (shading in Fig. 3a shows the response and black contours the TEKE climatology averaged over the last 20 years of the twentieth century). As noted in previous studies (Chang et al. 2012; Harvey et al. 2014; Lehmann et al. 2014; Harvey et al. 2020), wintertime North Atlantic TEKE is projected to strengthen mostly over the downstream region of the storm track and to a lesser extent over northeast America, and to slightly weaken at higher and lower latitudes. In particular, averaging the TEKE response over the downstream region of the storm track (green rectangle in Fig. 3a, where most of the intensification occurs) yields a multimodel mean strengthening of 9.56×10^4 J m^{-2} in TEKE (vertical black line in Fig. 3b). Note that 2 models, of the 14 models analyzed in this study, do not show any TEKE intensification over the downstream region of the storm track (gray bars in Fig. 3b). Nonetheless, the strengthening is clearly evident in the multimodel mean.

We next turn to isolate the role of ocean coupling in the intensification of wintertime North Atlantic TEKE using the
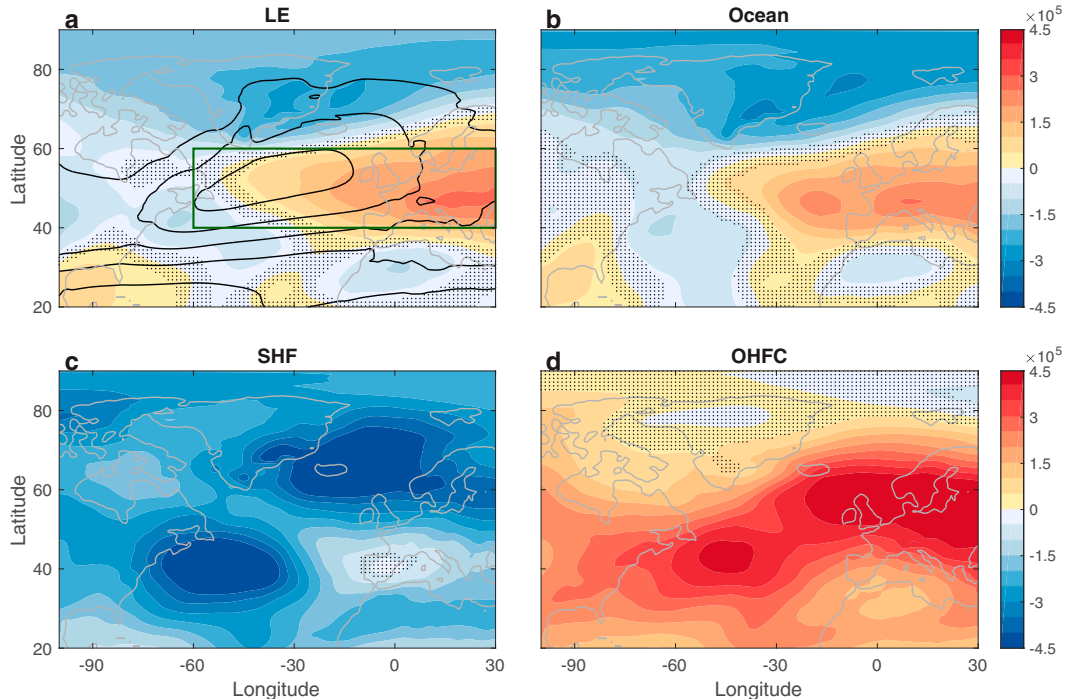
FIG. 4. (a) The response to anthropogenic emissions of DJF North Atlantic TEKE (J m^{-2}) in LE mean (shading). Black contours show the TEKE averaged over the last 20 years of the twentieth century in intervals of 5×10^5 J m^{-2}, with a maximum value of 3×10^6 J m^{-2}. The green-outlined box shows the downstream region of the storm track. The relative contribution to the response of the TEKE in LE from (b) ocean coupling (difference between LE and NOM LE), and from decomposing the ocean coupling to (c) thermodynamic coupling [surface heat fluxes (SHF); difference between SOM LE and NOM LE] and (d) dynamic coupling [ocean heat flux convergence (OHFC); difference between LE and SOM LE]. Stippling shows where the response is not statistically significant at the 5% level based on a Student's *t* test.

hierarchy of ocean coupling experiments in CESM1. Before analyzing the CESM1 ensembles, we first ensure that the projected forced response in LE is not an outlier within the CMIP5 models. The LE mean response of wintertime North Atlantic TEKE over the downstream region of the storm track (1.05×10^5 J m^{-2}; red line in Fig. 3b) is very similar to the CMIP5 mean response (cf. red and black lines), and thus is well within the response of the CMIP5 ensemble. This provides us confidence to use CESM1 for quantifying the role of ocean coupling in the future intensification of North Atlantic TEKE.

The spatial pattern of the North Atlantic TEKE response to anthropogenic emissions in the LE mean and the relative contributions from the different ocean coupling components are shown in Fig. 4. First, as in the CMIP5 mean (Fig. 3a), the LE mean exhibits a strengthening of North Atlantic TEKE mostly over the downstream region of the storm track, with a reduction at lower and higher latitudes (shading in Fig. 4a shows the response and black contours the TEKE climatology averaged over the last 20 years of the twentieth century). Unlike in the CMIP5 mean, the LE mean does not show a strengthening over northeast America, and the weakening at high latitudes is more robust; these responses thus might be model dependent. Nevertheless, the LE adequately simulates

the strengthening of the TEKE over the downstream region of the storm track as in the CMIP5 models. Second, isolating the role of ocean coupling in the TEKE response (i.e., taking the difference between LE and NOM LE; Fig. 4b) shows that ocean coupling accounts for most of the strengthening of North Atlantic TEKE over the downstream region of the storm track (in the absence of ocean coupling, i.e., in the NOM LE simulations, TEKE exhibits insignificant changes; Fig. S4a in the online supplemental material). This verifies the findings of Ciasto et al. (2016), who argued that the projected SST response by the end of this century accounts for most of the intensification of North Atlantic TEKE.

Given the important role of ocean coupling in the TEKE response we further decompose the ocean's contribution to thermodynamic coupling (i.e., the difference between SOM LE and NOM LE) and dynamic coupling (i.e., the difference between LE and SOM LE). While thermodynamic coupling (the effects of SHF) acts to weaken the North Atlantic TEKE by the end of this century (Fig. 4c), dynamic coupling (the effects of OHFC) acts to strengthen the TEKE (Fig. 4d). Thus, changes in OHFC are responsible for the intensification of North Atlantic TEKE; without changes in OHFC (i.e., in the SOM LE simulations) North Atlantic TEKE would have weakened by 2100, mostly, over the poleward and
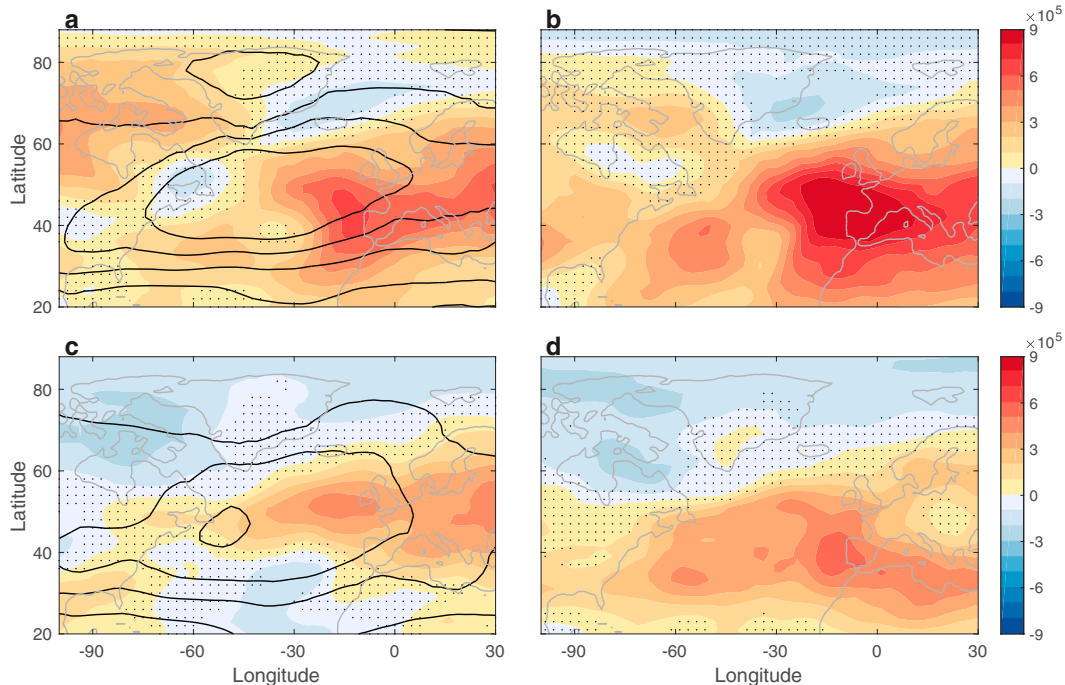
FIG. 5. The response to quadrupling of CO_2 concentrations, relative to preindustrial values, of DJF North Atlantic TEKE (J m^{-2}; shading) in (a) GISS Model E2.1 and (c) GFDL CM4. Black contours show the TEKE preindustrial climatology in intervals of 5×10^5 J m^{-2}, with a maximum value of 3×10^6 J m^{-2} in (a) and of 2.5×10^6 J m^{-2} in (c). Also shown is the relative contribution to the response of the TEKE from dynamic coupling (OHFC) in (b) GISS Model E2.1 and (d) GFDL CM4. Stippling shows where the response is not statistically significant at the 5% level based on a Student's t test.

equatorward flanks of the storm track (Fig. S4b in the online supplemental material).

Before further investigating the role of OHFC in the TEKE response, it is important to verify that the effect of OHFC to intensify the North Atlantic TEKE does not depend on the specific formulations of CESM1. We therefore next analyze the TEKE response in the fully coupled and slab ocean configurations of two other models: GISS Model E2.1 and GFDL CM4 (see the methods section). In both models we analyze the TEKE response to an abrupt quadrupling of CO_2 concentrations, relative to preindustrial values. We choose the abrupt $4 \times CO_2$ experiment, because it is expected to qualitatively yield similar results to the RCP8.5 experiment used in CESM1, where CO_2 levels are projected to approximately quadruple, relative to preindustrial values, by 2100.

First, similar to CESM1 and the CMIP5 mean (Figs. 4a and 3a), both GISS Model E2.1 (Fig. 5a) and GFDL CM4 (Fig. 5c) exhibit a strengthening of North Atlantic TEKE over the downstream region of the storm track under quadrupling of CO_2 concentrations (shading shows the response and black contours the TEKE preindustrial climatology). The pattern of this strengthening, however, is slightly different in these two models. While, similar to CESM1 and the CMIP5 mean, the strengthening of the TEKE in GFDL CM4 is confined to the downstream region of the storm track, in GISS Model E2.1 the strengthening is evident throughout the North Atlantic region. This suggests that

different models' configurations might affect the distribution of the TEKE response. Nonetheless, the strengthening over the downstream region of the storm track is clearly evident in both models.

Second, the role of OHFC in strengthening the TEKE in these models (evaluated by taking the difference between the TEKE response in the fully coupled and slab ocean configurations) is similar to the one projected in CESM1: OHFC accounts for most of the strengthening of North Atlantic TEKE over the downstream region of the storm track (Figs. 5b,d). Note that the role of OHFC in the TEKE response is larger in CESM1 in comparison with the GISS Model E2.1 and GFDL CM4 models. One explanation for this difference is the use of different forcings to evaluate the OHFC role. Indeed, under an abrupt $4 \times CO_2$ forcing, the role of OHFC in the TEKE response in CESM1 is similar to the OHFC role in the GISS Model E2.1 and GFDL CM4 models (Fig. S5 in the online supplemental material). Thus, the magnitude of the effect of OHFC to intensify the TEKE might vary across models and forcings. Nevertheless, the above analysis provides us confidence that the important role of changes in OHFC to drive the projected intensification of North Atlantic TEKE is robust and is not likely model dependent.

To quantify the roles of the different ocean coupling components in the TEKE response to anthropogenic emissions in CESM1 we next compare the averaged TEKE response over
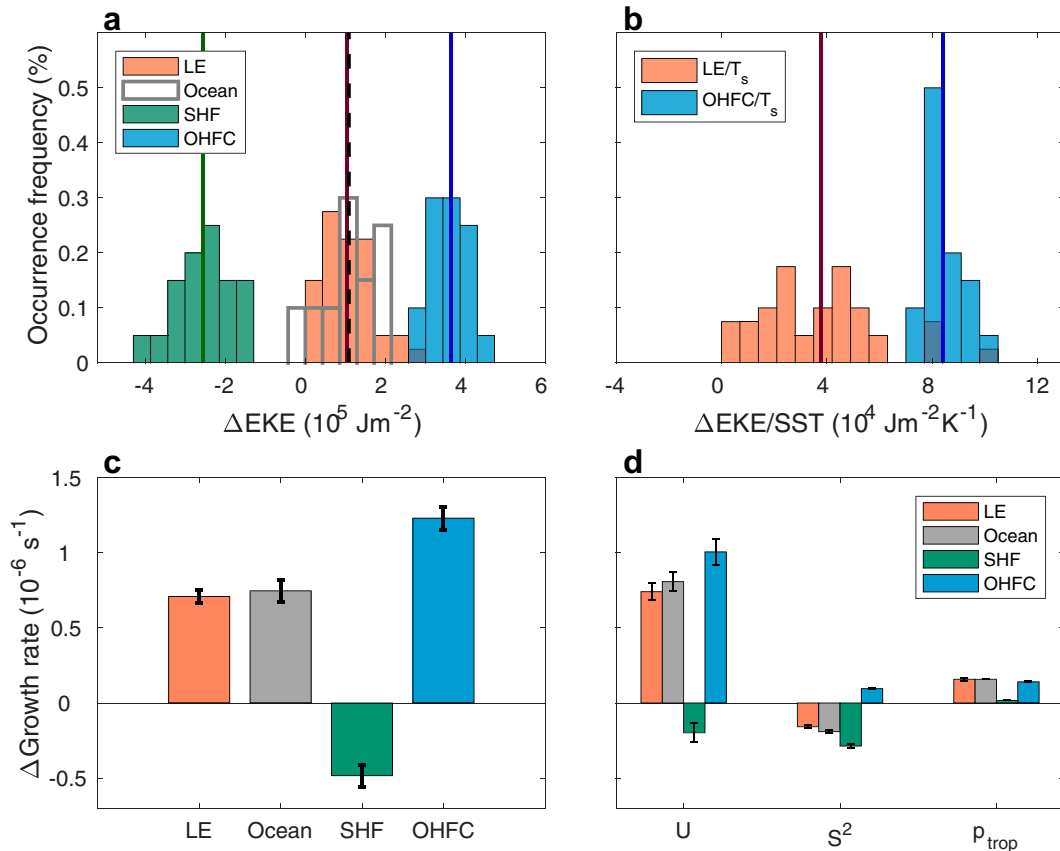
FIG. 6. (a) The occurrence frequency of DJF North Atlantic TEKE response to anthropogenic emissions (10^5 J m^{-2}) averaged over the downstream region of the storm track in LE (red bars). The relative contribution to the TEKE response from ocean coupling (gray-outlined bars) and from decomposing the ocean coupling to thermodynamic coupling (SHF; green bars) and dynamic coupling (OHFC; blue bars). Vertical red, dashed black, green, and blue lines show the LE mean response, mean ocean contribution, mean SHF contribution, and mean OHFC contribution, respectively. (b) The occurrence frequency of TEKE response normalized by the global mean SST response (10^4 J m^{-2} K^{-1}) in LE (red bars), and the relative contribution from dynamic coupling (OHFC; blue bars). Vertical red and blue lines show the LE mean response and mean OHFC contribution, respectively. (c) The growth-rate response (10^{-6} s^{-1}) in LE mean (red bar), and the relative contribution to the response of the growth rate from ocean coupling (gray bar) and from decomposing the ocean coupling to thermodynamic coupling (SHF; green bar) and dynamic coupling (OHFC; blue bar). (d) The relative contribution to the growth-rate response from the mean zonal wind u, static stability S^2, and tropopause height p_{trop} in LE (red bars), the contributions from ocean coupling (gray bars), thermodynamic coupling (SHF; green bars), and dynamic coupling (OHFC; blue bars). The error bars show the 95% confidence interval based on a Student's t distribution.

the downstream region of the storm track across the different ensembles (Fig. 6a). First, we consider the effects of total oceanic coupling. The TEKE intensification due to ocean coupling (1.09×10^5 J m^{-2}; vertical dashed black line) accounts for nearly all of the LE mean TEKE response (1.05×10^5 J m^{-2}; vertical red line). Thus, without ocean coupling North Atlantic TEKE is not expected to strengthen over the downstream region of the storm track. Further decomposing the ocean's contribution to thermodynamic (SHF; green bars) and dynamic (OHFC; blue bars) coupling shows that while changes in SHF act to weaken the North Atlantic TEKE by -2.55×10^5 J m^{-2} (vertical green line), changes in OHFC act to intensify the TEKE by 3.64×10^5 J m^{-2} (vertical blue line). Thus, North Atlantic TEKE is projected to intensify

by the end of the twenty-first century as the effect of SHF to weaken the TEKE is overcome by the large effect of OHFC to strengthen it.

The effects of OHFC on North Atlantic TEKE can be separated into the effects of net oceanic heat uptake by the deep ocean (i.e., global mean mixed layer OHFC) and of horizontal heat redistribution by ocean heat transport and nonuniform heat uptake (the difference between OHFC and net heat uptake). To disentangle these two processes, we next normalize the TEKE response by the global mean SST response. This normalization eliminates the role of net oceanic heat uptake by the deep ocean (i.e., global mean heat uptake) in delaying surface warming: the different global mean sea surface warming in LE and SOM LE is only due to changes in

net oceanic heat uptake by the deep ocean. Thus, the difference in the normalized TEKE response in LE and SOM LE isolates the contribution from horizontal heat redistribution. Figure 6b shows the TEKE response normalized by the global mean SST response in LE (red bars), along with the contribution from changes in horizontal heat redistribution (blue bars). Horizontal heat redistribution by ocean dynamics results in an intensification of 8.4×10^4 J m^{-2} K^{-1} (vertical blue line), which is 2.2 times the intensification, scaled by the global mean SST response, in LE (3.8×10^4 J m^{-2} K^{-1}; vertical red line). Since total OHFC results in an intensification that is 3.4 times the projected TEKE intensification in LE (blue and red bars in Fig. 6a), changes in horizontal heat redistribution account for almost two-thirds of the effect of ocean heat transport to intensify the North Atlantic TEKE; one-third of the intensification is due to changes in net oceanic heat uptake by the deep ocean.

The result that the intensification of North Atlantic TEKE is mostly due to changes in horizontal heat redistribution is different than the one reported in Woollings et al. (2012), where OHFC was argued to shift the storm track southward, with little effect on its intensity (cf. Fig. 3i in Woollings et al. 2012). As discussed in section 1, since the fully coupled and slab ocean models analyzed in Woollings et al. (2012) used different forcings (the 20C3M and SRESA1B forcing scenarios vs an idealized forcing of $2 \times CO_2$), their comparison not only isolates the role of ocean heat transport changes, but also the effects of the different external forcings used in these experiments (transient vs equilibrated forcings, with different CO_2 levels).

To further demonstrate the importance of using the same forcings across the different simulations in such an attribution analysis, we next investigate the role of OHFC in the projected TEKE intensification in LE using slab ocean model simulations under $2 \times CO_2$ and $4 \times CO_2$ forcings. First, as in Woollings et al. (2012), comparing the future TEKE response in LE with the response in the slab ocean model version of CESM1 under $2 \times CO_2$ forcing suggests that OHFC acts to reduce the TEKE intensity on the poleward flank of the storm track and increase the TEKE intensity on the equatorward flank, thus acting to shift the TEKE southward (Fig. S6a in the online supplemental material). Second, forcing the slab ocean model with an abrupt quadrupling of CO_2 concentrations, shows that the effect of OHFC to shift the storm track equatorward is significantly reduced, as OHFC acts to intensify the TEKE over most of the low–midlatitudes, with minor changes on the poleward flank of the storm track (Fig. S6b). Last, using the same forcings in both LE and the slab ocean model shows that OHFC does not contribute to the southward shift of the storms, but mostly intensifies the TEKE over the entire North Atlantic region (Fig. 4d, along with Fig. S6c).

The above analysis emphasizes that in order to adequately capture the role of OHFC it is critical to use the same forcings across the hierarchy of ocean coupling experiments. It is important to use not only the same magnitude of forcings, but also the same transient evolution of the forcing; the transient (over several years) and steady-state (over several decades) climate's responses to increased greenhouse gases were found

to be significantly different (Grise and Polvani 2017; Ceppi et al. 2018; Chemke and Polvani 2019). Last, we note that another difference that might contributes to the different TEKE responses in the CMIP3 slab ocean models analyzed in Woollings et al. (2012) and the SOM LE analyzed here is the representation of dynamic sea ice, which is active in SOM LE but not in all CMIP3 models (note that, as in SOM LE, thermodynamic sea ice models were present in all reported configurations of CMIP3 slab ocean models).

b. Elucidating the mechanism underlying the effects of ocean coupling on the future North Atlantic TEKE

Since winter midlatitude storm tracks are driven by baroclinic instability, investigating the future changes in the baroclinicity of the flow can provide meaningful insights on the projected storm tracks' response to anthropogenic emissions. In particular, we follow previous studies (e.g., Brayshaw et al. 2011; Frankignoul et al. 2013; Gastineau et al. 2013; Chemke and Polvani 2019; Chemke and Ming 2020) and investigate the fastest growth rate of the eddies, as a measure for baroclinicity. To calculate the growth rate of North Atlantic eddies we conduct a linear normal-mode instability analysis of the quasigeostrophic equations, linearized about the mean state of the downstream region of North Atlantic storm track (see the methods section). The analysis is conducted using the mean fields (zonal wind, static stability, and tropopause height), averaged over the last 20 years of the twentieth and twenty-first centuries, from each large ensemble.

First, in accordance with the intensification of North Atlantic TEKE by the end of this century, the growth rate of the waves in LE mean is also projected to increase (7.1×10^{-7} s^{-1}, red bar in Fig. 6c). Furthermore, ocean coupling increases the growth rate by 7.4×10^{-7} s^{-1} (gray bar in Fig. 6c), which demonstrates that, as for the TEKE intensity, having an active ocean results in the future increase of the eddies' growth rate. Second, decomposing the role of ocean coupling to thermodynamic and dynamic coupling shows that while thermodynamic coupling (SHF) acts to reduce the growth rate by the end of this century (-4.8×10^{-7} s^{-1}; green bar in Fig. 6c), dynamic coupling (OHFC) is responsible for the future increase in the growth rate (1.2×10^{-6} s^{-1}; blue bar in Fig. 6c). Thus, changes in the growth rate due to the different oceanic components are consistent with the effects of these oceanic components on the TEKE response to anthropogenic emissions. Note that the growth rate shows low correlation with the TEKE response across the different members in each ensemble, suggesting that the instability analysis might be insensitive to variations that arise from internal variability. Nevertheless, since here we focus on the role of ocean coupling in the forced response of TEKE, the above analysis provides us the confidence to investigate the growth rate changes to better understand the role of ocean coupling in the TEKE response.

The advantage of simplifying the North Atlantic storm-track behavior to an eigenvalue problem is that it allows one to isolate the role of the mean fields in the storm track's response to anthropogenic emissions. This is done by resolving Eq. (1) for the last 20 years of the twenty-first century
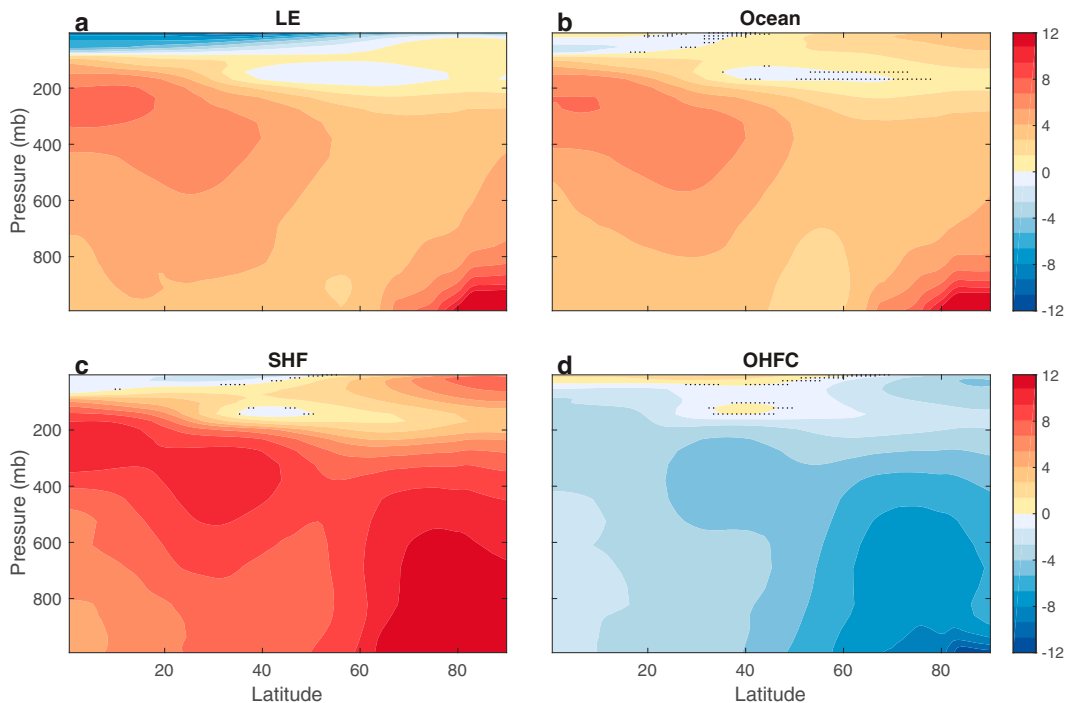
FIG. 7. As in Fig. 4, but for the mean temperature averaged over the downstream region of the storm track (60°W–30°E).

while keeping all mean fields at their last 20 years of the twentieth-century values except for one: the difference between the resulting growth rate and the growth rate of the last 20 years of the twentieth century isolates the role of each mean field in the growth-rate response to anthropogenic emissions. Figure 6d shows the relative contributions of the mean zonal wind, static stability, and tropopause height to the response of the growth rate of North Atlantic eddies across the different ensembles. First, the increase in the growth rate in LE (red bars) is due to changes in the zonal wind (7.4×10^{-7} s^{-1}). Changes in static stability, on the other hand, act to decrease the growth rate in LE, and thus to oppose its projected increase (-1.5×10^{-7} s^{-1}). Second, since ocean coupling (gray bars) is responsible for the increase in the growth rate (Fig. 6c), it also increases the growth rate via changes in the zonal wind (8.1×10^{-7} s^{-1}), and its effect on static stability acts to decrease the growth-rate response (-1.9×10^{-7} s^{-1}). Interestingly, while thermodynamic coupling (SHF, green bars) acts to reduce the growth-rate response via changes in both zonal wind (-1.9×10^{-7} s^{-1}) and static stability (-2.8×10^{-7} s^{-1}), dynamic coupling (OHFC, blue bars) overcomes the SHF tendency and acts to increase the growth rate via changes in the zonal wind (1×10^{-6} s^{-1}). The tropopause height has a minor contribution to the increase in the growth rate, mostly via OHFC changes.

To better understand the role of ocean coupling in the growth-rate response of North Atlantic eddies we next analyze the response of the mean temperature, averaged over the downstream region of the storm track (60°W–30°E), across the ensembles (Fig. 7). Changes in the temperature field hold information on both changes in the zonal wind shear (changes in the meridional temperature gradient), and changes in static stability (changes in the vertical temperature gradient). The North Atlantic temperature response in LE (Fig. 7a) is very similar to the global warming tropospheric temperature pattern of enhanced warming in the upper tropical troposphere, relative to the upper polar troposphere, and enhanced warming in the lower polar troposphere, relative to the lower tropical troposphere (i.e., Arctic amplification). These temperature changes have opposite effects on the baroclinicity of the flow. On one hand, they act to stabilize the troposphere at low to midlatitudes, and decrease the meridional temperature gradient at low levels, which act to reduce the baroclinicity. On the other hand, they act to destabilize the troposphere at high latitudes and increase the meridional temperature gradient aloft (along with the vertical wind shear; Fig. S7a in the online supplemental material), which increases the baroclinicity (Butler et al. 2010; Yuval and Kaspi 2020).

Ocean coupling accounts for most of the tropospheric temperature changes (and zonal wind changes; Fig. S7b in the online supplemental material) through all latitudes and levels (i.e., the warming of the upper tropical troposphere and Arctic amplification, Fig. 7b). This result is not surprising given that changes in surface temperature not only modify the warming of the upper tropical troposphere, by controlling the moist adiabatic lapse rate, but also modify Arctic amplification (Chemke et al. 2021), via surface feedbacks (e.g., albedo and Planck feedbacks). Indeed, in NOM LE, the absence of ocean coupling processes results in only minor atmospheric warming by 2100, mostly at low–midlatitudes, with no significant changes to the temperature gradients (Fig. 8a in the online supplemental material).
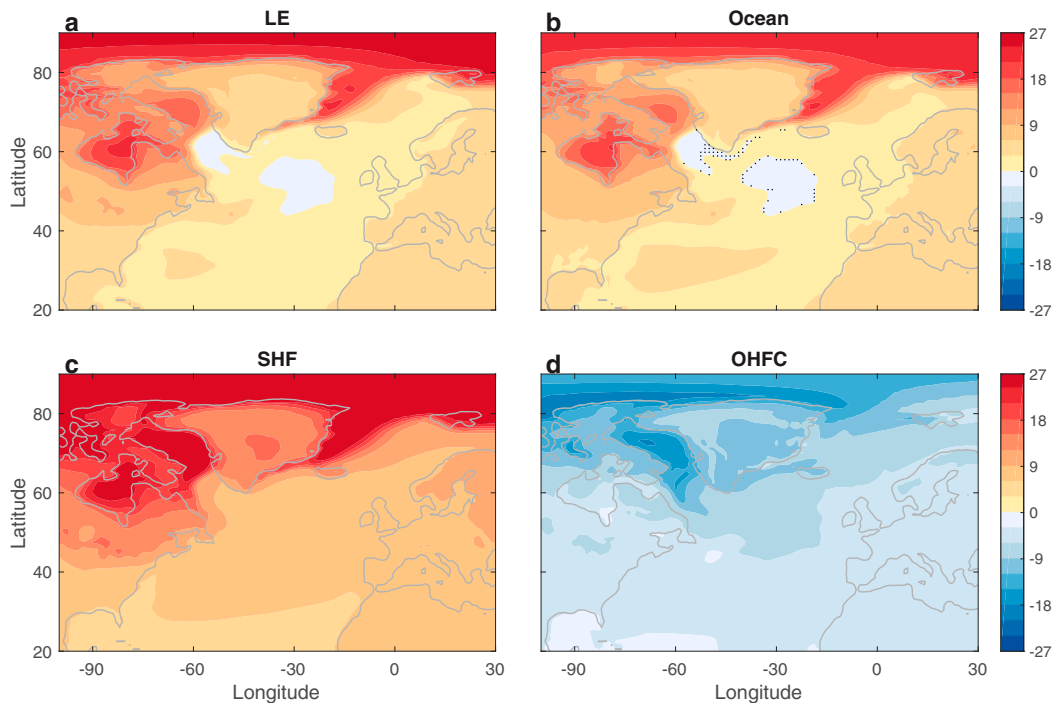
FIG. 8. As in Fig. 4, but for the surface temperature response (K).

Thermodynamic coupling (SHF; Fig. 7c) is not only responsible for the overall warming of the troposphere, but for the enhanced warming in the upper tropical troposphere, and for the Arctic amplification (Chemke et al. 2021). Thus, based on the growth-rate analysis in Fig. 6c, thermodynamic coupling acts to reduce the growth rate and the TEKE response by reducing the meridional temperature gradient over the low–midlevels (and the associated mean zonal wind shear at mid–high latitudes; Fig. S7c in the online supplemental material), and by stabilizing the troposphere at low–midlatitudes. Note that the opposite effects of thermodynamic coupling on the meridional temperature gradient at low and high levels (i.e., vertical variations in the wind shear) prevents simple metrics of baroclinicity, which assume constant wind shear and static stability, such as the Eady growth rate, from capturing the effects of thermodynamic coupling on the TEKE response; the effect of thermodynamic coupling on the Eady growth response strongly depends on which vertical levels are chosen for the analysis (Fig. S9 in the online supplemental material; using low levels seems to better capture the TEKE behavior; Hoskins and Valdes 1990; Gastineau and Frankignoul 2015).

Dynamic coupling (OHFC, Fig. 7d), on the other hand, acts to reduce the warming of the troposphere (via the increased heat uptake by the deep ocean), the Arctic amplification (Chemke et al. 2021), and the stratification of low to midlatitudes; in SOM LE, where OHFC changes are absent, the troposphere exhibits much stronger warming (due to the lack of increased ocean heat uptake by the deep ocean), with stronger Arctic amplification that is not confined to the surface but extends throughout the troposphere (Fig. S8b in the online supplemental material). Although dynamic coupling does not

overcome the effect of thermodynamic coupling to enhance the warming of the lower Arctic troposphere, and reduce the meridional temperature gradient at low levels, it substantially reduces the effects of thermodynamic coupling to warm the mid–upper polar troposphere, which results in an increase of the meridional temperature gradient aloft (and the associated mean zonal wind shear at mid–high latitudes; Fig. S7d in the online supplemental material). As discussed above, this effect of OHFC is due to both horizontal heat redistribution and net heat uptake by the deep ocean; since net heat uptake mitigates the warming of the surface, its cooling effect is also mostly evident over the Arctic, as it reduces the surface processes that result in Arctic amplification. Thus, by reducing the Arctic amplification (more than the upper tropical warming), OHFC increases the meridional temperature gradient (zonal wind shear) through most of the troposphere, which increases the baroclinicity (blue bars in Fig. 6d) and thus the TEKE intensity by the end of this century. Similar effects of DJF North Atlantic ocean coupling on Arctic amplification, were also found in the annual and zonal mean (Chemke et al. 2021). In particular, ocean coupling was found to account for ~80% of the Arctic amplification by the end of this century via thermodynamic coupling. In contrast, dynamic coupling was found to mitigate the Arctic warming and sea ice loss by ~35%.

Last, given that ocean coupling processes affect the TEKE response via changes in SST, we next examine the role of ocean coupling in the future response of the surface temperature to anthropogenic emissions. First, the surface temperature response in LE includes the strong warming of the Arctic, relative to lower latitudes, as well as the warming hole at midlatitudes (Fig. 8a). Second, similar to the atmospheric

temperature response, ocean coupling accounts for most of the surface temperature response (Fig. 8b); in NOM LE, the surface shows minor warming, even over the Arctic region (Fig. S10a in the online supplemental material). As a result, in NOM LE, the melting and variability of the Arctic sea ice are considerably reduced (Fig. S11 in the online supplemental material).

Decomposing the effect of ocean coupling on the surface temperature shows that thermodynamic coupling acts to warm the surface throughout the North Atlantic, but more at high latitudes than low latitudes, thus resulting in the Arctic amplification (Fig. 8c). This effect of thermodynamic coupling acts to reduce the surface (and lower troposphere) meridional temperature gradient (which is also evident in the SOM LE simulations; Fig. S10b in the online supplemental material) and thus to reduce the growth rate and the TEKE response. Consistently, previous studies showed that an increase in the surface meridional temperature gradient, over the Gulf Stream region, acts to intensify the storm track (Brayshaw et al. 2011).

Investigating the SHF response to anthropogenic emissions (Fig. S12 in the online supplemental material), where positive (negative) values indicate a heat flux into (out of) the ocean, reveals that similar to the effect of thermodynamic coupling on the surface temperature, the SHF act to warm the North Atlantic SST over mid–high latitudes, and to increase oceanic heat loss to the Arctic sea ice, which enhances the wintertime Arctic sea ice loss and amplification (Screen and Simmonds 2010). These two processes support the thermodynamic coupling tendency to reduce the meridional temperature gradient. Further decomposing the effects of the SHF shows that sensible and latent heat fluxes are mostly responsible for warming of the North Atlantic, and, together with longwave radiative fluxes, they act to enhance the Arctic oceanic heat loss (Fig. S13 in the online supplemental material).

In contrast, dynamic coupling acts to cool the surface (Fig. 8d). The overall cooling by dynamic coupling is due to the effects of net ocean heat uptake by the deep ocean; in the absence of OHFC the surface considerably warms in SOM LE, with no evidence for the North Atlantic warming hole (Chemke et al. 2020) (Fig. S10b in the online supplemental material). The cooling by dynamic coupling is stronger at high latitudes than low latitudes, which acts to oppose the effect of thermodynamic coupling to reduce the meridional temperature gradient (Fig. 7d). As discussed above, this effect of dynamic coupling is evident throughout the polar troposphere leading to the intensification in baroclinicity and in TEKE by 2100.

c. The role of ocean coupling in the spread of the projected TEKE response

The different responses of North Atlantic TEKE to anthropogenic emissions across CMIP5 models (gray bars in Fig. 3b) could arise from both the different models' formulations, and from the internal climate variability. In LE, on the other hand, the different TEKE responses across the LE members only stem from the internal climate variability. While the LE

mean shows a similar intensification of the TEKE to the CMIP5 mean intensification (cf. red and black lines in Fig. 3b), the spread across the LE members (3.9×10^9 J^2 m^{-4}, defined as the variance of the TEKE response across the LE members; Fig. 6a) is approximately one-quarter of the spread across CMIP5 models (1.6×10^{10} J^2 m^{-4}, Fig. 3b). Thus, assuming that the spread of the TEKE response across the LE members is similar in other ensembles of CMIP5 models (and that the ensemble members are independent of the different models' formulations, i.e., that their covariance is zero), ~25% of the spread in the TEKE response across CMIP5 models is due to internal variability while the other ~75% is due to the different formulations of CMIP5 models.

Given the important role of ocean coupling in the forced response of the TEKE to anthropogenic emission, we next assess the effect of ocean coupling on the spread of the TEKE response in LE. The spread in the TEKE response in NOM LE (i.e., with no ocean coupling) of 4.9×10^9 J^2 m^{-4} captures all of the spread across the LE members (cf. red and gray bars in Fig. 6a). Thus, while ocean coupling has an important role in driving the forced response of the TEKE to anthropogenic emissions, it has a mitigating effect on the spread of the TEKE response in LE (i.e., on its internal variability). Interestingly, the LE was found to underestimate part of the multidecadal variability in North Atlantic oceanic processes (Kim et al. 2018). Thus, while it is conceivable that the internal variability, estimated from the LE, should have explained a larger portion of the CMIP5 spread, the minor effect of ocean coupling on the internal variability in LE suggests that the multidecadal ocean variability biases in LE are less likely to affect the above result.

As discussed in section 1, Woollings et al. (2012) suggested, using correlation analysis, that the different weakening of AMOC across CMIP3 models might explain half of the spread in the storm track's response across the models. Here, on the other hand, since the ocean has a relatively small effect on the spread across the LE members, the weakening of AMOC [defined, following Woollings et al. (2012), as the maximum value of the annual mean Atlantic meridional streamfunction at 45°] and the TEKE response are poorly correlated across the ensemble members, with $r = -0.07$ (Fig. 9). We argue that any previously suggested effects of AMOC weakening on the spread of the storm track's response across different models are not likely due to internal variability, but due to the different models' formulations. Namely, the different surface temperature responses to anthropogenic emissions across the models (i.e., the different models' sensitivity) might result in the different AMOC and TEKE responses (Todd et al. 2020).

4. Summary

Previous studies have argued for the importance of ocean–atmosphere coupling, and in particular of dynamic coupling (OHFC changes), in the projected response of the North Atlantic storm track to anthropogenic emissions. However, to date, the roles of ocean coupling and its different components in modifying the storm track's response are not fully understood.
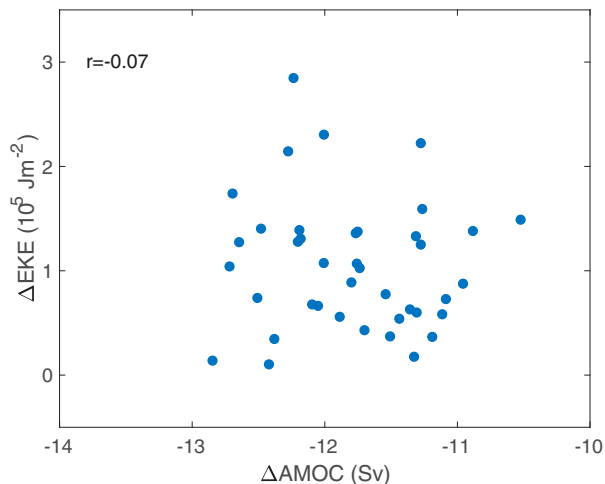
FIG. 9. The response to anthropogenic emissions of DJF North Atlantic TEKE (10^5 J m^{-2}) averaged over the downstream region of the storm track as a function of the AMOC response (Sv; 1 Sv $\equiv$ 10^6 m^3 s^{-1}) in LE. Their correlation appears in the upper-left corner.

Using the CESM1 we construct a hierarchy of ocean coupling experiments (including fully coupled, fixed OHFC and fixed SST configurations) in large ensembles of model simulations forced across the twentieth and twenty-first centuries under the historical and RCP8.5 forcings. Such a hierarchy not only allows us to isolate and quantify the role of ocean coupling in the North Atlantic TEKE response, but also to further decompose the role of ocean coupling to thermodynamic ocean coupling (the effects of surface heat fluxes) and dynamic coupling (the effects of OHFC). We find that by the end of this century ocean coupling accounts for nearly all of the strengthening of North Atlantic TEKE over the downstream region of the storm track. While surface heat fluxes act to weaken the TEKE by the end of this century, OHFC changes overcome this weakening effect, and are found to be responsible for the intensification of North Atlantic TEKE. Further decomposing the role of OHFC changes reveals that horizontal heat redistribution by ocean heat transport and nonuniform heat uptake accounts for two-thirds of the effect of OHFC to intensify the TEKE, while one-third is due to the effect of net oceanic heat uptake by the deep ocean to delay surface warming.

Investigating the mechanism underlying the effect of ocean coupling on North Atlantic TEKE reveals that ocean coupling intensifies the TEKE by modulating the zonal wind shear. In particular, OHFC changes increase the meridional temperature gradient (i.e., zonal wind shear) in the middle-to-upper troposphere, by reducing the Arctic amplification (i.e., the larger warming of the Arctic relative to lower latitudes), which increases the growth rate of North Atlantic eddies, and intensifies the TEKE. In addition, we show that while ocean coupling is responsible for the forced intensification of North Atlantic TEKE, it has a relatively minor effect on the internal variability (intermember spread) of the TEKE response. Thus, any previously suggested roles of AMOC weakening in

explaining the spread in the storm track's response across the models is not likely due to internal variability but might solely stem from the effect of the different models' formulations (i.e., different surface temperature response) on the AMOC response (Todd et al. 2020).

Last, given that the strengthening of North Atlantic TEKE is found to arise from OHFC changes, it is important to elucidate which OHFC processes are responsible for intensifying the TEKE. While the answer to this question is beyond the scope of this paper, the low correlation between the intensification of the TEKE and the weakening of AMOC across the LE members suggests that the wind-driven circulation might play an important role in the intensification of the TEKE (Woollings et al. 2012).

REFERENCES

Bellomo, K., M. Angeloni, S. Corti, and J. von Hardenberg, 2021: Future climate change shaped by inter-model differences in Atlantic meridional overturning circulation response. *Nat. Commun.*, **12**, 3659, https://doi.org/10.1038/s41467-021-24015-w.

Bitz, C. M., K. M. Shell, P. R. Gent, D. A. Bailey, G. Danabasoglu, K. C. Armour, M. M. Holland, and J. T. Kiehl, 2012: Climate sensitivity of the Community Climate System Model, version 4. *J. Climate*, **25**, 3053–3070, https://doi.org/10.1175/JCLI-D-11-00290.1.

Brayshaw, D. J., B. Hoskins, and M. Blackburn, 2011: The basic ingredients of the North Atlantic storm track. Part II: Sea surface temperatures. *J. Atmos. Sci.*, **68**, 1784–1805, https://doi.org/10.1175/2011JAS3674.1.

Butler, A. H., D. W. J. Thompson, and R. Heikes, 2010: The steady-state atmospheric circulation response to climate change–like thermal forcings in a simple general circulation model. *J. Climate*, **23**, 3474–3496, https://doi.org/10.1175/2010JCLI3228.1.

Ceppi, P., G. Zappa, T. G. Shepherd, and J. M. Gregory, 2018: Fast and slow components of the extratropical atmospheric circulation response to CO$_2$ forcing. *J. Climate*, **31**, 1091–1105, https://doi.org/10.1175/JCLI-D-17-0323.1.

Chang, E. K. M., Y. Guo, and X. Xia, 2012: CMIP5 multimodel ensemble projection of storm track change under global warming. *J. Geophys. Res.*, **117**, D23118, https://doi.org/10.1029/2012JD018578.

Chemke, R., 2021: Future changes in the Hadley circulation: The role of ocean heat transport. *Geophys. Res. Lett.*, **48**, e2020GL091372, https://doi.org/10.1029/2020GL091372.

——, and L. M. Polvani, 2018: Ocean circulation reduces the Hadley cell response to increased greenhouse gases. *Geophys. Res. Lett.*, **45**, 9197–9205, https://doi.org/10.1029/2018GL079070.

——, and ——, 2019: Exploiting the abrupt 4 × CO₂ scenario to elucidate tropical expansion mechanisms. *J. Climate*, **32**, 859–875, https://doi.org/10.1175/JCLI-D-18-0330.1.

——, and Y. Ming, 2020: Large atmospheric waves will get stronger, while small waves will get weaker by the end of the 21st century. *Geophys. Res. Lett.*, **47**, e2020GL090441, https://doi.org/10.1029/2020GL090441.

——, L. M. Polvani, and C. Deser, 2019: The effect of Arctic Sea ice loss on the Hadley circulation. *Geophys. Res. Lett.*, **46**, 963–972, https://doi.org/10.1029/2018GL081110.

——, L. Zanna, and L. M. Polvani, 2020: Identifying a human signal in the North Atlantic warming hole. *Nat. Commun.*, **11**, 1540, https://doi.org/10.1038/s41467-020-15285-x.

——, L. M. Polvani, J. E. Kay, and C. Orbe, 2021: Quantifying the role of ocean coupling in Arctic amplification and sea-ice loss over the 21st century. *npj Climate Atmos. Sci.*, **3**, 46, https://doi.org/10.1038/s41612-021-00204-8.

Ciasto, L. M., C. Li, J. J. Wettstein, and N. G. Kvamstø, 2016: North Atlantic storm-track sensitivity to projected sea surface temperature: Local versus remote influences. *J. Climate*, **29**, 6973–6991, https://doi.org/10.1175/JCLI-D-15-0860.1.

Coumou, D., J. Lehmann, and J. Beckmann, 2015: The weakening summer circulation in the Northern Hemisphere mid-latitudes. *Science*, **348**, 324–327, https://doi.org/10.1126/science.1261768.

Czaja, A., C. Frankignoul, S. Minobe, and B. Vanniere, 2019: Simulating the midlatitude atmospheric circulation: What might we gain from high-resolution modeling of air-sea interactions? *Curr. Climate Change Rep.*, **5**, 390–406, https://doi.org/10.1007/s40641-019-00148-5.

Deser, C., A. Phillips, V. Bourdette, and H. Teng, 2012: Uncertainty in climate change projections: The role of internal variability. *Climate Dyn.*, **38**, 527–546, https://doi.org/10.1007/s00382-010-0977-x.

——, L. Sun, R. A. Tomas, and J. Screen, 2016: Does ocean coupling matter for the northern extratropical response to projected Arctic sea ice loss? *Geophys. Res. Lett.*, **43**, 2149–2157, https://doi.org/10.1002/2016GL067792.

Frankignoul, C., G. Gastineau, and Y. Kwon, 2013: The influence of the AMOC variability on the atmosphere in CCSM3. *J. Climate*, **26**, 9774–9790, https://doi.org/10.1175/JCLI-D-12-00862.1.

Gastineau, G., and C. Frankignoul, 2015: Influence of the North Atlantic SST variability on the atmospheric circulation during the twentieth century. *J. Climate*, **28**, 1396–1416, https://doi.org/10.1175/JCLI-D-14-00424.1.

——, F. D'Andrea, and C. Frankignoul, 2013: Atmospheric response to the North Atlantic Ocean variability on seasonal to decadal time scales. *Climate Dyn.*, **40**, 2311–2330, https://doi.org/10.1007/s00382-012-1333-0.

Gervais, M., J. Shaman, and Y. Kushnir, 2019: Impacts of the North Atlantic warming hole in future climate projections: Mean atmospheric circulation and the North Atlantic jet. *J. Climate*, **32**, 2673–2689, https://doi.org/10.1175/JCLI-D-18-0647.1.

Grise, K. M., and L. M. Polvani, 2017: Understanding the time scales of the tropospheric circulation response to abrupt CO₂ forcing in the Southern Hemisphere: Seasonality and the role

of the stratosphere. *J. Climate*, **30**, 8497–8515, https://doi.org/10.1175/JCLI-D-16-0849.1.

Harvey, B. J., L. C. Shaffrey, and T. J. Woollings, 2014: Equator-to-pole temperature differences and the extra-tropical storm track responses of the CMIP5 climate models. *Climate Dyn.*, **43**, 1171–1182, https://doi.org/10.1007/s00382-013-1883-9.

——, P. Cook, L. C. Shaffrey, and R. Schiemann, 2020: The response of the Northern Hemisphere storm tracks and jet streams to climate change in the CMIP3, CMIP5, and CMIP6 climate models. *J. Geophys. Res.*, **125**, e32701, https://doi.org/10.1029/2020JD032701.

Held, I. M., and Coauthors, 2019: Structure and performance of GFDL's CM4.0 climate model. *J. Adv. Model. Earth Syst.*, **11**, 3691–3727, https://doi.org/10.1029/2019MS001829.

Hoskins, B. J., and P. J. Valdes, 1990: On the existence of storm-tracks. *J. Atmos. Sci.*, **47**, 1854–1864, https://doi.org/10.1175/1520-0469(1990)047<1854:OTEOST>2.0.CO;2.

Hurrell, J. W., and Coauthors, 2013: The Community Earth System Model: A framework for collaborative research. *Bull. Amer. Meteor. Soc.*, **94**, 1339–1360, https://doi.org/10.1175/BAMS-D-12-00121.1.

Kay, J. E., and Coauthors, 2015: The Community Earth System Model (CESM) Large Ensemble project: A community resource for studying climate change in the presence of internal climate variability. *Bull. Amer. Meteor. Soc.*, **96**, 1333–1349, https://doi.org/10.1175/BAMS-D-13-00255.1.

Kelley, M., and Coauthors, 2020: GISS-E2.1: Configurations and climatology. *J. Adv. Mod. Earth Syst.*, **12**, e2019MS002025, https://doi.org/10.1029/2019MS002025.

Kim, W. M., S. Yeager, P. Chang, and G. Danabasoglu, 2018: Low-frequency North Atlantic climate variability in the Community Earth System Model Large Ensemble. *J. Climate*, **31**, 787–813, https://doi.org/10.1175/JCLI-D-17-0193.1.

Lehmann, J., D. Coumou, K. Frieler, A. V. Eliseev, and A. Levermann, 2014: Future changes in extratropical storm tracks and baroclinicity under climate change. *Environ. Res. Lett.*, **9**, 084002, https://doi.org/10.1088/1748-9326/9/8/084002.

Magnusdottir, G., C. Deser, and R. Saravanan, 2004: The effects of North Atlantic SST and sea ice anomalies on the winter circulation in CCM3. Part I: Main features and storm track characteristics of the response. *J. Climate*, **17**, 857–876, https://doi.org/10.1175/1520-0442(2004)017<0857:TEONAS>2.0.CO;2.

O'Gorman, P. A., and T. Schneider, 2008: Energy in midlatitude transient eddies in idealized simulations of changed climates. *J. Climate*, **21**, 5797–5806, https://doi.org/10.1175/2008JCLI2099.1.

Riahi, K., and Coauthors, 2011: RCP 8.5—A scenario of comparatively high greenhouse gas emissions. *Climatic Change*, **109**, 33–57, https://doi.org/10.1007/s10584-011-0149-y.

Screen, J. A., and I. Simmonds, 2010: Increasing fall-winter energy loss from the Arctic Ocean and its role in Arctic temperature amplification. *Geophys. Res. Lett.*, **37**, L16707, https://doi.org/10.1029/2010GL044136.

Smith, K. S., 2007: The geography of linear baroclinic instability in earth's oceans. *J. Mar. Res.*, **65**, 655–683, https://doi.org/10.1357/002224007783649484.

Taylor, K. E., R. J. Stouffer, and G. A. Meehl, 2012: An overview of CMIP5 and the experiment design. *Bull. Amer. Meteor. Soc.*, **93**, 485–498, https://doi.org/10.1175/BAMS-D-11-00094.1.

Todd, A., and Coauthors, 2020: Ocean-only FAFMIP: Understanding regional patterns of ocean heat content and dynamic sea level change. *J. Adv. Model. Earth Syst.*, **12**, e02027, https://doi.org/10.1029/2019MS002027.

Woollings, T., J. M. Gregory, J. G. Pinto, M. Reyers, and D. J. Brayshaw, 2012: Response of the North Atlantic storm track to climate change shaped by ocean-atmosphere coupling. *Nat. Geosci.*, **5**, 313–317, https://doi.org/10.1038/ngeo1438.

Yuval, J., and Y. Kaspi, 2020: Eddy activity response to global warming-like temperature changes. *J. Climate*, **33**, 1381–1404, https://doi.org/10.1175/JCLI-D-19-0190.1.

Zappa, G., L. C. Shaffrey, K. I. Hodges, P. G. Sansom, and D. B. Stephenson, 2013: A multimodel assessment of future projections of North Atlantic and European extratropical cyclones in the CMIP5 climate models. *J. Climate*, **26**, 5846–5862, https://doi.org/10.1175/JCLI-D-12-00573.1.